INFLUENCE OF SCALE INTERACTIONS ON POLLUTANT VENTILATION MECHANISMS IN A TURBULENT STREET CANYON

Maxime Tan-Sicat
Institut de Mécanique des Fluides de Toulouse
Université de Toulouse, CNRS, INPT, UPS
Toulouse, France
maxime.sicat@imft.fr

Romain Mathis
Institut de Mécanique des Fluides de Toulouse
Université de Toulouse, CNRS, INPT, UPS
Toulouse, France
romain.mathis@imft.fr

Frédéric Y. Moulin
Institut de Mécanique des Fluides de Toulouse
Université de Toulouse, CNRS, INPT, UPS
Toulouse, France
frederic.moulin@imft.fr

Sébastien Cazin
Institut de Mécanique des Fluides de Toulouse
Université de Toulouse, CNRS, INPT, UPS
Toulouse, France
sebastien.cazin@imft.fr

Yara Abidine
Institut de Mécanique des Fluides de Toulouse
Université de Toulouse, CNRS, INPT, UPS
Toulouse, France
yara.abidine@imft.fr

Jean Dominique Barron
Institut de Mécanique des Fluides de Toulouse
Université de Toulouse, CNRS, INPT, UPS
Toulouse, France
jeandominique.barron@imft.fr

INTRODUCTION

Proper understanding of pollutant ventilation mechanisms in city streets is important for the prediction and management of air quality. To this effect, we investigate the canonical configuration of the street canyon, which has been the subject of dispersion studies in the past (Caton *et al.*, 2003; Ahmad *et al.*, 2005) and is considered a good model representative of the most common features of real-life streets. Yet, a comprehensive understanding of the interaction between the roughness sub-layer (RSL) and the canyon has not been achieved. This knowledge would be valuable for evaluated and predicted exchanges of heat, mass and momentum between the canopy and the above atmosphere. It is now well established that in wall bounded flows numerous processes are driven by scale interactions (Smits *et al.*, 2011), and particularly that the large-scale structures influence significantly the near-wall flow which has been evidence in smooth boundary layers by Mathis *et al.* (2009), and later studied in the urban boundary layer by Basley *et al.* (2018), Blackman *et al.* (2018) and Blackman *et al.* (2019).

In this study, we aim to investigate the scale interactions between the outer flow and the canyon. Special attention is given to analysing their impact on dispersion and ventilation processes, and how results are influenced by the canyon geometry. For this purpose, we have developed a dedicated experiment for two street canyon geometries, one narrow and one large, representative of the most encountered regimes : the skimming flow regime and the wake-interference regime (Oke, 1988), respectively. Measurements combine particle image velocimetry (PIV) and planar laser-induced fluorescence (PLIF). The convergence of large- and small-scale events above and within the canyon has been achieved through the use of high resolution measurements in both temporal and spatial terms, as detailed in the next section.

EXPERIMENTAL DETAILS

Experiments were conducted in the 22 m long hydraulic flume at the *Institut de Mécanique des Fluides de Toulouse* described in Chagot *et al.* (2020). The test section is $B = 1.10$ m wide and $D = 0.50$ m high, giving an aspect ratio $B/D = 3.1$. Downstream of a flow-conditioning section, the boundary layer develops over a 16 m fetch covered with regularly spaced cubic roughness elements of height $h = 40$ mm. The cubes are arranged in an aligned pattern with equal spacings $W = 51$ mm, yielding a planar packing density $\lambda_p = 20\%$, defined as $\lambda_p = A_p/A_T$, where A_p is the roughness plan area and A_T the total bed area. This configuration falls within the wake-interference regime described by Oke (1988) and was selected to emulate an urban-like turbulent boundary layer.

An idealized street canyon is modelled by two spanwise square bars of same height h as the upstream cubes, extending across the channel width (Fig.1b). Two cases are considered: a narrow canyon ($h/W = 1.25$), representative of skimming flow regime, and a wide canyon ($h/W = 3.55$), corresponding to a wake-interference regime similar to the upstream roughness (Oke, 1988). Downstream, the final 5 m section is again covered with the same cubic roughness. The coordinate system (x, y, z) denotes the streamwise, spanwise, and vertical directions, with the origin at the upstream bottom corner of the canyon. Velocity components (u, v, w) and scalar concentration c use overbars for time averages and primes for fluctuations.

Simultaneous velocity and scalar measurements were per-

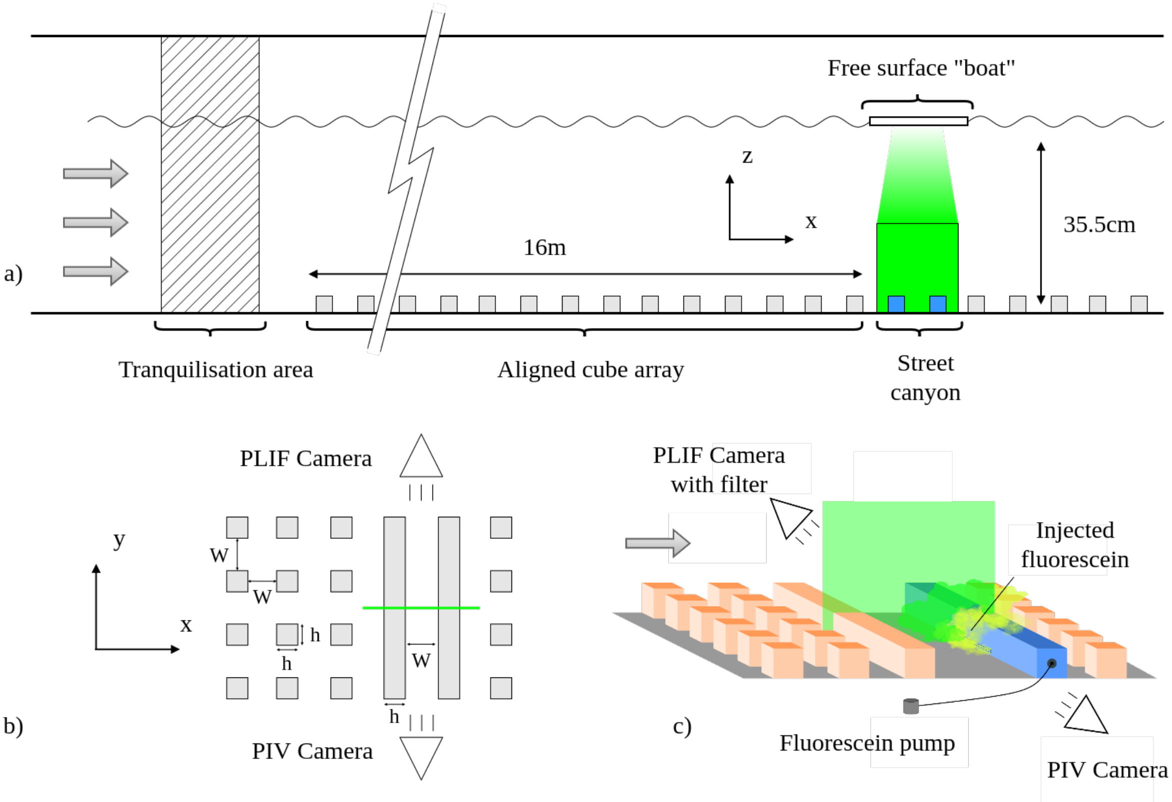

Figure 1. (a) Hydraulic flume experimental setup. (b) Disposition of aligned cube roughness elements and street canyon bars with respect to cameras and laser sheet. (c) Fluorescein injection setup for PLIF measurements.

Table 1. Main experimental characteristics.

U_e $(m.s^{-1})$	u_*/U_e	δ/h	Re_h	Re_δ
0.40	0.078	6	1 200	7 200

formed to examine canyon ventilation across scales. Data was acquired at 25 Hz for about 60 minutes per configuration, ensuring adequate convergence and temporal resolution of turbulent structures. Velocity fields were obtained by Particle Image Velocimetry (PIV) and scalar concentration by Planar Laser-Induced Fluorescence (PLIF). The shared field of view extends up to $4h$ in height, with widths of $3h$ (narrow canyon) and $3.6h$ (wide canyon). The outer velocity U_e was estimated by extrapolating a logarithmic profile from prior laser doppler velocimetry measurements.

The two-component velocity fields in the (x,z) plane at the channel centerline were measured using a LaVision PIV system. A 16-bit sCMOS camera (2560×2160 pixels) with a 60 mm Nikkor lens ($f_\# = 22$) was positioned laterally (Fig. 1c), while illumination was provided from above by a Litron dual-cavity 532 nm Nd:YAG laser delivering 2×200 mJ per pulse. To limit free-surface distortions, the laser sheet passed through a glass interface. The flow was seeded with 10 μm glass microbeads in a closed loop. A total of 90,000 image pairs were recorded at 25 Hz over 60 minutes, with a 5 ms inter-frame delay. Processing with DaVis employed a multi-pass adaptive scheme (window sizes from 96×96 to 16×16 pixels, 75% overlap), yielding a spatial resolution of about 0.32 mm. False vectors were detected and removed using a median filter.

The scalar transport was studied using fluorescein as a passive tracer. A 25 mg/L solution was injected through a 200 mm $\times$ 10 mm array of 1 mm holes spaced 1 mm apart, located at the base of the partially hollow downstream bar (Fig. 1c), at a constant flow rate of 4 mL/s supplied by a gear pump. PLIF measurements used a second 16-bit sCMOS camera (same resolution) with a 60 mm Nikkor lens ($f_\# = 2.8$), positioned opposite the PIV system and equipped with an optical filter isolating fluorescein emission. Intensities were converted to concentration via a linear calibration. Spatial variations in laser-sheet intensity were corrected using a reference image obtained after uniformly filling the flume with fluorescein, enabling pixel-wise normalization (Torres *et al.*, 2013).

FREQUENCY ANALYSIS

The frequency content of the flow is analyzed to identify the relevant scales involved. Figure 2 shows streamwise evolution of the pre-multiplied spectra of the concentration fluctuations at the canyon interface ($z = h$), where $x = 0$ correspond to the upstream edge of the canyon. In the narrow canyon case spectra is relatively homogeneous along the canyon length and seems to exhibit two different scales: a large-scale component at $f\delta/U_e \leq 0.1$ and a smaller-scale component around $1 \leq f\delta/U_e \leq 3$. The large canyon case exhibits a somewhat similar dichotomy in the initial third of the canyon, before the apparition of intermediate frequencies in the middle of the canyon, with the lower frequencies reappearing close to the downstream bar. These low-frequency signatures reveal the influence of large-scale motions present in rough turbulent boundary layer, as described by Cameron *et al.* (2017) and Perret & Kerhervé (2019). However, their frequency range is insufficiently well defined. Basley *et al.* (2018) reported cutoff frequencies f^{co} between large- and small-scales in ur-

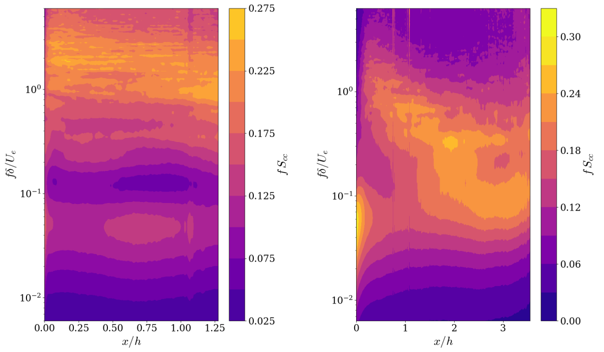

Figure 2. Evolution of the pre-multiplied spectra of the concentration at the canyon interface $z = h$. Left: Narrow canyon configuration ; Right: Large canyon configuration

ban boundary layers within the range of $0.2 \le f^{co}\delta/U_e \le 0.5$ (where δ is the boundary layer thickness and U_e the free-stream velocity). Pre-multiplied spectra of the scalar concentration fluctuations across the canyon interface at $z = h$ in figure 2 suggest scale-separation at the lower end of this range.

In order to identify the influence of the large-scale motions of the roughness sublayer, we look at the spectral coherence between the streamwise velocity component at ($x = W/2$, $z = 4h$) and the streamwise velocity component u, the wall-normal velocity component w and the concentration c at the center of the canyon interface ($x = W/2$, $z = h$). The spectral coherence $\gamma^2_{xy}(f)$ measures the correlation between two signals $x(t)$ and $y(t)$ at a given frequency f, defined as (Bendat & Piersol, 1971)

$$\gamma^2_{xy}(f) = \frac{|S_{xy}(f)|^2}{S_{xx}(f)S_{yy}(f)}, \quad (1)$$

where S_{xy} and S_{xx} are the cross and auto-spectra, respectively. Results are shown in figure 3 for both canyons. In both cases, the outer signal u_{4h} depicts a good coherence with u_{1h} and c_{1h} at low-frequency, whereas no coherence exists with w_{1h}. This allows us to estimate a cutoff frequency $f^{co}\delta/U_e \approx 0.09$, which is somewhat lower than the values reported by Basley *et al.* (2018), possibly due to the difference in boundary layer thickness to building height ratio δ/h.

SCALE DECOMPOSITION

In this section we take a closer look at the interactions between the different scales of flow using a triple decomposition of the velocity and scalar fields. First, we use the Reynolds decomposition to separate the mean and fluctuating components. Then, the fluctuating part is decomposed in the Fourier space into large- and small-scale components using a low-pass butterworth filter at the cutoff frequency f^{co} identified above, as following

$$\begin{aligned} u_{4h}(t) &= \overline{u}_{4h} + u'_{4h,LS}(t) + u'_{4h,SS}(t), \\ w_{1h}(t) &= \overline{w}_{1h} + w'_{1h,LS}(t) + w'_{1h,SS}(t), \\ c_{1h}(t) &= \overline{c}_{1h} + c'_{1h,LS}(t) + c'_{1h,SS}(t), \end{aligned} \quad (2)$$

where $\overline{\cdot}$ and $.'$ indicate mean and fluctuating components, respectively. Subscripts LS and SS indicate the large- and the small-scale content, respectively.

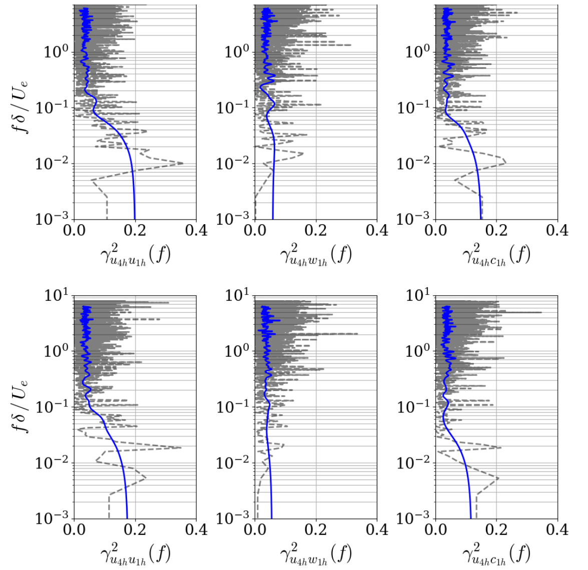

Figure 3. Spectral coherence γ^2 between the outer streamwise velocity component u_{4h} and u_{1h}, w_{1h} and c_{1h}. A smoothed curve (in blue) is overlaid over the raw coherence (in grey). Top: narrow canyon ; Bottom: large canyon.

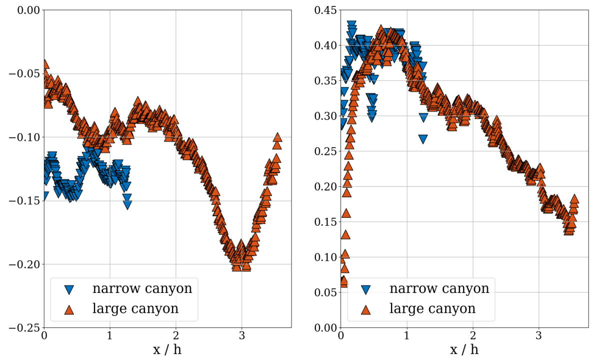

Figure 4. Amplitude modulation coefficient (as defined by Equation 3) depending on position along the canyon interface. Left: $AM_c = AM\left[u'_{4h,LS}, c'_{1h,SS}(x)\right]$; Right: $\mathrm{AM}_w = AM\left[u'_{4h,LS}, w'_{1h,SS}(x)\right]$

Finally, we quantify the degree of amplitude modulation of the outer large-scales onto near-canopy small-scales flow using the procedure given by Mathis *et al.* (2009).

$$AM_c = AM\left[u'_{4h,LS}, c'_{1h,SS}\right] = \frac{\overline{u'_{4h,LS} E_L\left[c'_{1h,SS}\right]}}{\sqrt{\overline{u'^2_{4h,LS}}}\sqrt{\overline{E^2_L\left[c'_{1h,SS}\right]}}} \quad (3)$$

where $E_L\left[c'_{1h,SS}\right]$ is the large-scale component of the envelope of the small-scale signal considered (either c' or w'), defined as

$$E_L\left[c'_{1h,SS}\right] = \mathrm{lowpass}\left(\mathscr{H}\left[c'_{1h,SS}\right]\right). \quad (4)$$

Figure 4 shows the streamwise evolution of AM_c and AM_w along the canyon interface ($z = h$). In both cases, a negative

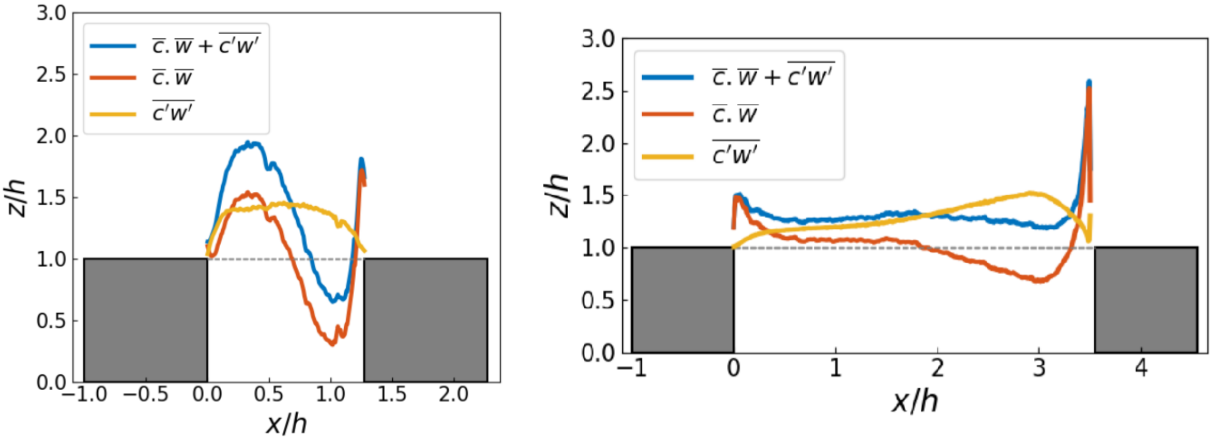

Figure 5. Scalar transport along the canyon interface, total, mean and turbulent. Left: narrow canyon ; Right: Large canyon.

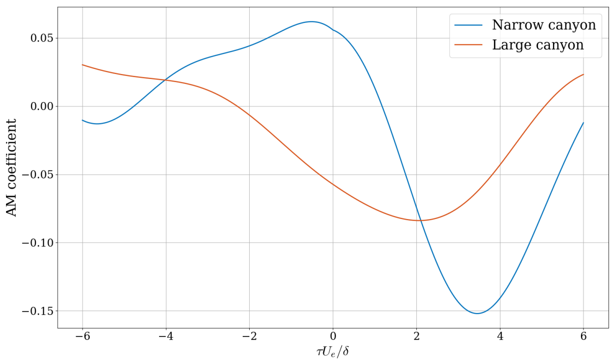

Figure 6. Amplitude modulation coefficient of the turbulent vertical scalar exchange Φ_t by the large scales $u_{4h,LS}$

amplitude modulation coefficient AM_c is noticed, whereas a positive occurs for the AM_w. There is a stark contrast in the spatial evolution between the narrow and the large canyons. In the narrow canyon, AM_c stays almost constant across the interface with little oscillations ($AM_c \simeq 0.13 \pm 0.02$). In the large canyon, AM_c have similar behavior for the first half, before plunges to a extrema of -0.2 at $x/h = 3$. Position $x/h = 3$ is also the location of maximum turbulent scalar exchange along the interface (red curve in Fig. 5, right). This is probably due to the proximity of the downstream bar in front of which scalar accumulates before being ejected from the canyon. When a large, low-momentum turbulent structure passes over, it favors the ejection of pollutant from the canyon, hence the negative modulation. The amplitude modulation of the vertical velocity fluctuations by the large scales at $z = h$ is positive in both canyons, $AM_w \simeq 0.4$ for $x/h \leq 1.25$. This large amplitude modulation could be attributed to the modulation by the passing large scales of flow separation above the upstream bar. In the large canyon configuration the amplitude modulation AM_w decreases steadily from $x/h = 1.25$ until the downstream canyon edge. Figure 5 portrays the total, mean and turbulent transport at the interface ($z = h$). It shows that the ventilation mechanisms and spatial distribution differ significantly between the two canyons, which is consistent with the *AM* coefficient profiles shown in figure 4.

To further analyse those differences, we examine the total turbulent scalar exchange across the canyon interface Φ_t, as defined

$$\Phi_t(t) = \int_{x=0}^{W} c'(x, z = h, t) w'(x, z = h, t) dx. \qquad (5)$$

Its amplitude modulation coefficient is shown in figure 6 against the reduced time delay $\tau U_e/\delta$. The negative peak of *AM*, occurring at a positive time delay in both cases, indicates that low-momentum structures drive the ejection of scalar from the canyon. This peak is slightly more pronounced in the narrow canyon, suggesting that ventilation at the interface is more sensitive to large-scale effects than in the large canyon.

CONCLUSION

Synchronized 2D2C PIV and PLIF measurements were conducted on two street canyon geometries in order to study interactions between the outer flow and the canyon interface, as well as to investigate their influence on the canyon ventilation. Significant differences were found between the narrow and large street canyon configurations. While the narrow canyon, in a "skimming flow" regime, tends to exhibit relatively symmetric flow characteristics along its interface at $z = h$, the large canyon, in a "wake-interference flow" regime, exhibits asymmetry between the upstream and downstream corners. Influence of the large turbulent scales of the flow at $z = 4h$ and the canyon interface at $z = h$ were investigated through the study of amplitude modulation mechanisms. It was found that the large outer scales strongly modulate the small scales at the interface, such as the vertical velocity fluctuations $w'(t)$, hence $c'(t)$, but differently for the two canyon configurations. Further studies would allow for a deeper investigation into these differences and their underlying mechanisms.

REFERENCES

Ahmad, K., Khare, M. & Chaudhry, K.K. 2005 Wind tunnel simulation studies on dispersion at urban street canyons and intersections—a review. *Journal of Wind Engineering and Industrial Aerodynamics* **93** (9), 697–717.

Basley, Jérémy, Perret, Laurent & Mathis, Romain 2018 Spatial modulations of kinetic energy in the roughness sublayer. *Journal of Fluid Mechanics* **850**, 584–610.

Bendat & Piersol 1971 *Random Data: Analysis and Measurement Procedures*. John Wiley & Sons, Inc.

Blackman, Karin, Perret, Laurent & Calmet, Isabelle 2018 Energy transfer and non-linear interactions in an urban boundary layer using Stochastic Estimation. *Journal of Turbulence* **19** (10), 849–867.

Blackman, Karin, Perret, Laurent & Mathis, Romain 2019 Assessment of inner–outer interactions in the urban boundary layer using a predictive model. *Journal of Fluid Mechanics* **875**, 44–70.

Cameron, S. M., Nikora, V. I. & Stewart, M. T. 2017 Very-large-scale motions in rough-bed open-channel flow. *Journal of Fluid Mechanics* **814**, 416–429.

Caton, F., Britter, R.E. & Dalziel, S. 2003 Dispersion mechanisms in a street canyon. *Atmospheric Environment* **37** (5), 693–702.

Chagot, Loïc, Moulin, Frédéric Y. & Eiff, Olivier 2020 Towards converged statistics in three-dimensional canopy-dominated flows. *Experiments in Fluids* **61** (24).

Mathis, Romain, Hutchins, Nicholas & Marusic, Ivan 2009 Large-scale amplitude modulation of the small-scale structures in turbulent boundary layers. *Journal of Fluid Mechanics* **628**, 311–337.

Oke, T R 1988 Street design and urban canopy layer climate. *Energy and Buildings* .

Perret, Laurent & Kerhervé, Franck 2019 Identification of very large scale structures in the boundary layer over large roughness elements. *Experiments in Fluids* **60** (6).

Smits, Alexander J., McKeon, Beverley J. & Marusic, Ivan 2011 High–reynolds number wall turbulence. *Annual Review of Fluid Mechanics* **43** (Volume 43, 2011), 353–375.

Torres, Luis A., Fleck, Brian A., Wilson, David J. & Nobes, David S. 2013 Calibration of a planar laser induced fluorescence technique for use in large scale water facilities. *Measurement* **46** (8), 2597–2607.